



Article

Surface Preparation for Coating and Erosion MRR of SS 304 Using Silicon Carbide Abrasive Jet

Deb Kumar Adak^{1,2}, Vivekananda Pal¹, Santanu Das¹ , Tina Ghara³, Hillol Joardar⁴, Nashmi Alrasheedi⁵ and Barun Haldar^{5,*} 

¹ Kalyani Government Engineering College, Kalyani 741235, West Bengal, India

² Mechanical Engineering Department, College of Engineering and Management, Kolaghat 721171, West Bengal, India

³ Mechanical Engineering Department, Indian Institute of Technology, Kharagpur 721302, West Bengal, India

⁴ Mechanical Engineering Department, C V Raman Global University, Bhubaneswar 752054, Odisha, India

⁵ Mechanical and Industrial Engineering Department, College of Engineering, Imam Mohammad Ibn Saud Islamic University (IMSIU), Riyadh 11432, Saudi Arabia

* Correspondence: dr.barun.haldar@gmail.com

Abstract: The surface preparation of shiny stainless steels is a must for applying esthetic paints, effective functional plasma spray coating, laser cladding, welding, etc., applications. The current work aims for effective surface roughening and erosion MRR of SS 304 work surface using SiC abrasive jet erosion and optimization of the process parameters. The response surface approach is used to design and conduct the studies using the Box–Behnken design method. The surface topography of the eroded surfaces is examined by a 2D profilometer, 3D profilometer, and scanning electron microscope (SEM). The abrasive grit size and working gas pressure greatly affect the surface roughness of SS 304 samples. The influence of the process parameters on the variation of these topographical features is analyzed and confirmed. The working jet pressure is seen to significantly impact erosion MRR. The lower working gas pressure shows a typical influence on R_a (surface preparation) and as pressure increases, erosion MRR rises, and the surface preparation mode shifts to the erosion metal removal/cutting zone. The quality of SS 304 surface prepared from SiC abrasive jet impact is characterized by 3D profilometry.



Citation: Adak, D.K.; Pal, V.; Das, S.; Ghara, T.; Joardar, H.; Alrasheedi, N.; Haldar, B. Surface Preparation for Coating and Erosion MRR of SS 304 Using Silicon Carbide Abrasive Jet. *Lubricants* **2023**, *11*, 10. <https://doi.org/10.3390/lubricants11010010>

Received: 13 November 2022

Revised: 11 December 2022

Accepted: 22 December 2022

Published: 28 December 2022



Copyright: © 2022 by the authors. Licensee MDPI, Basel, Switzerland. This article is an open access article distributed under the terms and conditions of the Creative Commons Attribution (CC BY) license (<https://creativecommons.org/licenses/by/4.0/>).

Keywords: abrasive wear; surface preparation; abrasive jet erosion; abrasive jet machining; grit blasting; characterization; material removal rate (MRR)

1. Introduction

The abrasive jet blasting is effectively used in surface cleaning and surface preparation simultaneously for mechanical interlocking with a coating material. Moreover, the abrasive jet has multipurpose applications in pre-processing (surface preparation, cleaning, dry etching, etc.), main processing (drilling, cutting operations, surface hardening, etc.), and post-processing (hard surface removal of casting surface, dry polishing, deburring). The material removal using an abrasive jet is caused by erosion [1,2] and provides several benefits, such as the ability to produce roughly smoothed surface finishes and cut ductile to brittle and heat-sensitive delicate materials safely. An abrasive jet is mostly used to machine brittle materials more effectively since it is flexible and produces less heat. Additionally, the abrasive jet system carries out various distinctive tasks including micro-machining and polishing the surface of micro-channels and holes.

Surface preparation is a prerequisite to different processes like cladding, thermally spraying, brazing, painting, etc. In an experiment involving vacuum brazing of stainless steel, Hebda et al. [2] concluded that surfaces needed to be prepared with a roughness value (R_a) ranging from 0.24 μm to 0.68 μm before brazing. Surface preparations of Inconel 625 and 718 for improved wettability were studied by Lankiewicz et al. [3] using SiC of

sizes 120 μm and 220 μm . They recorded R_a values of 0.96 μm and 0.98 μm . Another classic application of the abrasive jet process is the removal of damaged paint and simultaneously preparing the surface for the re-painting of bridges, ships, automobiles, etc. Surface area and surface energy both rise as roughness rises after the impingement of abrasive particles on the substrate surface. For an improved bonding between the substrate surface and the coating material during coating application, a rough surface is required for a larger gripping area and bonding contact points [4]. According to Melentiev et al. [5], the abrasive jet system shifted from a macro- to a micro-zone after continuous development. An abrasive jet was used to clean the rusty and greasy surface of the substrate before welding since it is quicker and more effective than other surface cleaning procedures like grinding, filing, etching, and so on [1]. Additionally, AJM was carried out using an effective dust-collecting system, which allows for smooth operation and the elimination of environmental loading issues [1–5]. In contrast to AWJM, which cannot successfully operate at low pressure as indicated by Akkurt et al. [6], the abrasive jet can perform under low pressure on thinner materials. To find out the present status and research gaps, the search and review of present investigators on surface preparation using abrasive jet and allied processes are tabulated in Table 1.

Table 1. Surface preparation on various engineering materials using abrasive erosion jets.

Process	Work Material	Abrasive	Process Details and Parameters	Results	Source
Grit Blasting	Low carbon steel, C45 steel, SS316, Ti-6Al-4V, Inconel 718 and Hastelloy X	Al_2O_3 (704 μm)	<ul style="list-style-type: none"> ■ Nozzle impact angle: 90°, SOD: 120 mm, blasting time: 60 sec, jet pressure: 7 bar. 	<ul style="list-style-type: none"> ■ R_a: 3.34 to 3.70 μm. ■ Johnson-Cook flow stress correlates with maximum compressive stress. 	Ghara et al., 2020 [7]
Grit Blasting	Low carbon steel, Ti-6Al-4V, Inconel 718	Al_2O_3 (704 μm)	<ul style="list-style-type: none"> ■ Jet pressure: 5 to 8 bar, nozzle impact angle: 20 to 90°, SOD: 60 to 140, blasting time: 5 to 15 s. 	<ul style="list-style-type: none"> ■ R_a: 2.5 to 4 μm (Low carbon steel); R_a: 2.5 to 3.5 μm (Ti-6Al-4V); R_a: 2.8 to 3.7 μm (Inconel 718). 	Ghara et al., 2020 [8]
AWJM	MS	SiO_2 (80 mesh)	<ul style="list-style-type: none"> ■ Transverse speed: 85 to 567 mm/min; flow rate: 390 to 450 gm/min; ■ SOD: 3 to 7 mm. 	<ul style="list-style-type: none"> ■ R_a: 0.53 μm. ■ Traverse speed is the foremost significant factor. 	Parikshit et al., 2018 [9]
AJM	MS	Al_2O_3 (12–50 μm), SiC (25, 50 μm)	<ul style="list-style-type: none"> ■ Flow rate: 15 gm/min. ■ velocity: 200 m/s. 	<ul style="list-style-type: none"> ■ R_a: 0.012 μm (using Al_2O_3); R_a: 0.013 μm (using SiC); R_a: 0.018 mm (un-machined piece). 	Chaitanya et al., 2019 [10]
AJP	SKD61 mould steel	SiC (800 mesh)	<ul style="list-style-type: none"> ■ Traverse speed: 100 to 200 mm/s; ■ nozzle dia.: 4 mm, impact angle: 30 to 60°, SOD: 10 to 20 mm.; ■ blasting time: 3 min, jet pressure: 2 to 4 kg/cm². 	<ul style="list-style-type: none"> ■ R_a: 1.03 to 0.13 μm. ■ Pure water: Water solvent machine oil = 1:1, reduce the cutting force and a mirror-like polished surface can be obtained. 	Tsai et al., 2007 [11]
Abrasive blasting	MS	Steel (450 μm , Al_2O_3 (450 μm)	<ul style="list-style-type: none"> ■ Jet pressure: 0.7 MPa; ■ SOD: 300 mm. ■ nozzle impact angle: 30, 60, and 90°; ■ machining time 5 s; ■ abrasive flow rate 3.83 L/min. 	<ul style="list-style-type: none"> ■ R_a: 9.22–9.74 μm (using steel grit); R_a: 8.49–8.81 μm (using Al_2O_3 grit). ■ R_a value is maximum for 90° impact angle. 	Kim et al., 2021 [12]
Grit blasting	MS	Al_2O_3 (24–60 μm)	<ul style="list-style-type: none"> ■ Nozzle impact angle: 20 to 90°, SOD: 50 to 200 mm; ■ jet pressure: 5 and 7 bar, blasting time 15 to 180 s. 	<ul style="list-style-type: none"> ■ R_a: 2.5 to 6 μm. ■ Compressive residual stress increases with blasting pressure and blasting angle. 	Chander et al., 2009 [13]
Shot blasting	S275 carbon steel	Corundum (630 μm), Glass spheres (425 μm)	<ul style="list-style-type: none"> ■ Pressure: 1 to 5 bar; ■ SOD 100 mm; ■ Impact angle 90°. 	<ul style="list-style-type: none"> ■ R_f: 15 to 35 μm. ■ Increase in pressure has a greater impact on erosion. 	Banon et al., 2020 [14]

Table 1. Cont.

Process	Work Material	Abrasive	Process Details and Parameters	Results	Source
Sandblasting	EN AW 2024 T3 aluminium alloy	Garnet 80 E+	<ul style="list-style-type: none"> ■ Jet pressure: 300 to 700 KPa; ■ SOD: 40 to 155 mm; ■ Speed of sample displacement 50 to 100 mm/min. 	<ul style="list-style-type: none"> ■ S_a: 0.82 to 1.58 μm. ■ R_a: 0.79 to 1.52 μm. ■ R_z: 6.64 to 12.16 μm. 	Baranska et al., 2021 [15]
AHAJM	soda-lime glass	SiC (100 μm)	<ul style="list-style-type: none"> ■ Feed rate: 20 to 40 mm/min; ■ SOD: 4 to 12 mm; ■ work temperature 27 to 320 °C. 	<ul style="list-style-type: none"> ■ R_a: 1.37 to 3.05 μm, ■ Temperature influences AHJM process. 	Jagannatha et al., 2012 [16]
FB-HAJM	hard stone quartz	hot SiC (275 μm)	<ul style="list-style-type: none"> ■ Nozzle: AISI D2 steel, SOD: 4 to 8 mm; ■ jet pressure: 3 to 7 Kgf/cm². 	<ul style="list-style-type: none"> ■ R_z: 0.941 to 1.545 μm. ■ Optimal nozzle life 80 h is predicted by genetic algorithm (GA) and validated. 	Pradhan et al., 2020 [17]
AJM	borosilicate glass	Al ₂ O ₃ (25–150 μm)	<ul style="list-style-type: none"> ■ Nozzle: speed 2 mm/s, dia.: 1.5 mm. SOD: 10 mm. 	<ul style="list-style-type: none"> ■ R_a: 0.80 to 2.36. ■ Smooth surface formed with low impact angle. 	Jafar et al., 2013 [18]
AJM	soda-lime glass	SiC (300–850 μm)	<ul style="list-style-type: none"> ■ Jet pressure: 3 to 5 kg/cm². ■ SOD: 4 to 12 mm. 	<ul style="list-style-type: none"> ■ R_a: 2.22 to 6.65 μm. ■ Taguchi and WPCA can improve MRR and surface roughness. 	Nayak et al., 2017 [19]
AJM	glass fibre reinforced polymer	SiC (50–130 μm)	<ul style="list-style-type: none"> ■ Nozzle: hardened steel, dia. 1.5 to 3.5 mm, operating angle 90°, SOD: 0.5 to 2.5 mm; ■ jet pressure: 2 to 6 bar. 	<ul style="list-style-type: none"> ■ R_a: 0.531 μm (threaded nozzle), 0.802 μm (plain nozzle) ■ Whirling effect can improve surface roughness. 	Madhu et al., 2018 [20]
AJM	Alumina	Green SiC (800 mesh)	<ul style="list-style-type: none"> ■ Jet pressure: 0.3 MPa; ■ SOD: 0.5 mm. ■ table feed: 05 mm/s. 	<ul style="list-style-type: none"> ■ R_z: 0.5 μm. ■ Strength improves (~15%). 	Wakuda et al., 2002 [21]
FM-AJM	Al6061	SiC (100–200 μm)	<ul style="list-style-type: none"> ■ Nozzle: dia. 4 mm; ■ magnetic field intensity: 40 milli-gauss; ■ machining time 20 s. ■ jet pressure: 0.4 and 0.6 MPa; ■ SOD: 50 and 70 mm. ■ impact angle: 30 and 45°. 	<ul style="list-style-type: none"> ■ R_a: 1.36 μm. ■ Better surface roughness than traditional machining with slip scratch effect. 	Jiuag-Hung et al., 2012 [22]
AJM	Aluminium	SiO ₂ (0.35 to 1.6 mm)	<ul style="list-style-type: none"> ■ Jet pressure: 0.6 MPa. 	<ul style="list-style-type: none"> ■ R_z: 15.65 to 46.89 μm. 	Slatineanu et al., 2018 [23]
μ -AJM	Aluminium 6061 alloy	SiC, Al ₂ O ₃	<ul style="list-style-type: none"> ■ Jet Pressure: 25 to 100 KPa, ■ SOD: 30 mm. 	<ul style="list-style-type: none"> ■ R_a: 0.70 to 2 μm. 	Kyu Kwon et al., 2022 [24]
AWJM	AISI 304 SS	SiC	<ul style="list-style-type: none"> ■ Flow rate: 250–350 gm/min; ■ nozzle dia.: 0.3 mm, ■ traverse speed 100–150 mm/min ■ SOD: 1–2 mm. ■ water jet pressure: 3400–3200 bar. 	<ul style="list-style-type: none"> ■ R_a: 4.328 to 5.120 μm. ■ kerf taper observed: 1.72~2.23°. 	Sanghani et al., 2017 [25]
PAWAJM	AISI 4140 alloy steel	Al ₂ O ₃ (58 μm)	<ul style="list-style-type: none"> ■ Feed rate: 0.1 mm/rev; ■ width of cut 3 mm, ■ cutting speed 300 m/min. 	<ul style="list-style-type: none"> ■ R_a: 14 to 56 μm. 	Wang et al., 2020 [26]
AWJM	AISI 304	GMT garnet (80 mesh)	<ul style="list-style-type: none"> ■ Jet pressure 350 MPa; ■ flow rate 475 to 571; ■ traverse speed 48 to 417 (mm/min). 	<ul style="list-style-type: none"> ■ R_a: 2.13 to 2.98 μm. 	Ficko et al., 2021 [27]
AWJM	C45, 37MnSi5, 30CrV9 steel	Australian garnet (80 mesh)	<ul style="list-style-type: none"> ■ Jet pressure 380 MPa; ■ abrasive flow rate 225 g/min; ■ SOD: 2 mm; ■ traverse speed 100 mm/min. 	<ul style="list-style-type: none"> ■ R_a: 1.2 to 2 μm (C45); ■ R_a: 0.70 to 2.5 μm (37MnSi5); ■ R_a: 0.8 to 1.6 μm (30CrV9). 	Hlavacova et al., 2020 [28]

In this present search and review on abrasive jet surface preparation, it was observed that SiC and Al₂O₃ are mostly used as abrasives for the surface preparation of various metal surfaces. SiO₂ is also used, which is cheaper, but easily broken into pieces on impact. For multiple-times usage and cost-effectiveness, SiC is one of the best choices for surface preparation and abrasive machining, eventually providing hard sharp edges with long service life. In most of the surface preparation studies, prepared roughness R_a values vary from 0.5 to 4 μm , and in some cases, it was observed around 10 μm , and more than 50 μm . Generally, micro-roughening (etching) would be good for precision applications like wetting of the surface, mechanical interlocking in PVD, CVD coatings, and painting applications. A highly rough surface would be effective in plasma spray coating, laser cladding, bulk coating, etc.

Stainless steel (SS) is the second most useful alloy after steel [29], and among all grades of SS, SS 304 is mostly used (58% of total use of SS in 2004) [30] in industries. It has huge applications in machinery, sheet metal working, medical, food production, automotive, tank, vessel, etc., and manufacturing industries. Therefore, there is a huge demand for machining, surface preparation, joining, forming, and processing of SS 304. Search and review (Table 1) show that surface preparation of SS/SS 304 might be rarely practiced using an abrasive jet process.

The present study aims to investigate abrasive jet surface preparation in the roughening mechanism and the influence of process parameters on both surface topography/characteristics of SS 304 and erosion MRR . The experiments were conducted by an in-house developed abrasive jet system which has unique characteristics like abrasive flow and mixing ratio (carrier gas: abrasive) control ability. The air pressure, stand-off distance, abrasive grain size, and abrasive flow rate are chosen as input parameters and responses are mainly observed in roughness (R_a) and material removal rate. The Box–Behnken design approach is adopted for the experiment design, analysis, optimization, and validation. In addition, response surface methodology (ANOVA) is applied to understand the interrelationship between the process parameters and the responses. Furthermore, important surface characteristics like sharpness and density of peaks present on the prepared surface are investigated and discussed thoroughly for surface characterization.

2. Materials and Methods

An indigenously designed and made abrasive jet system, as shown in Figure 1a insert of the main machining unit and Figure 1b workpiece adjustment with the nozzle, was utilized for surface preparation on 1 mm thick SS 304 sheets of surface $\sim(6 \times 3) \text{ mm}^2$. The chemical composition (revealed by laser spectroscopy) of the used SS 304 samples is given in Table 2 below.

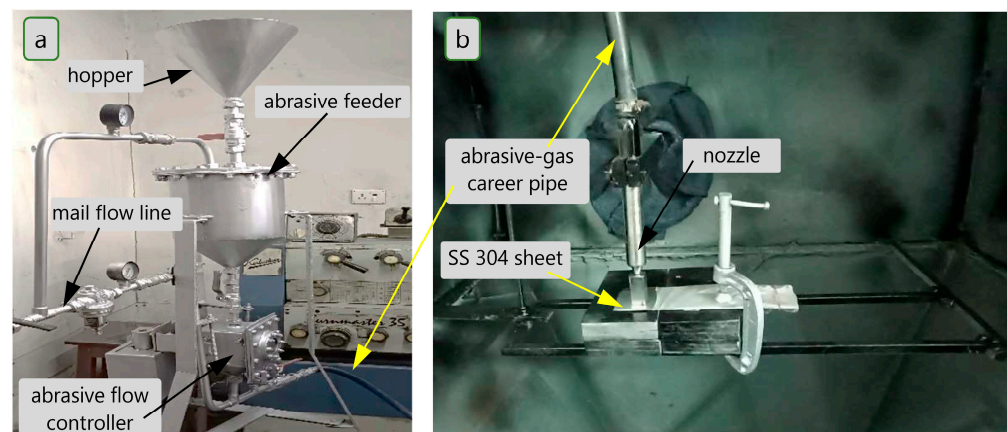
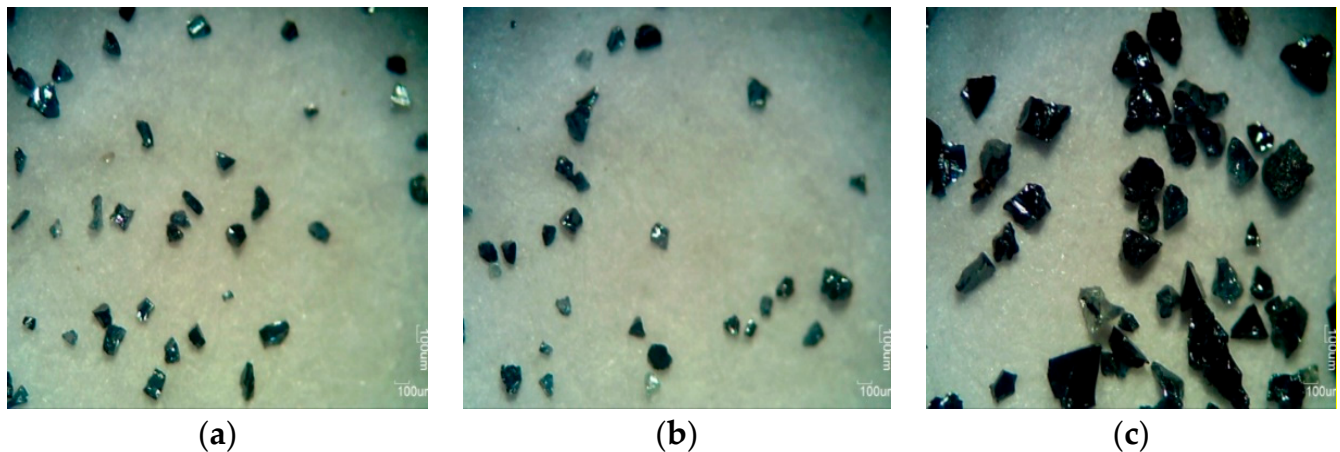


Figure 1. The insert photography of (a) the main machining unit, and (b) workpiece adjustment with the nozzle.

Table 2. Chemical composition of used SS 304.

Elements	Fe	C	Si	Mn	P	S	Cr	Ni	Cu	V	W	B
Average wt. %	69.400	0.0217	0.377	1.54	0.0216	0.0023	19.30	8.890	0.027	0.141	0.015	0.004

The setup was fabricated in the Manufacturing Technology Laboratory of Kalyani Government Engineering College, West Bengal, India, with the help of Asian Drilling Industries, a Kolkata-based company. Silicon carbide (SiC) grits of 100, 150, and 200 μm sizes (Figure 2a, Figure 2b and Figure 2c, respectively) are used for the experiment. A commercial stainless-steel nozzle with a 4 mm opening diameter was used for the present investigation. Mild steel stand pieces measuring 24, 28, and 30 mm were used for the accurate measurement of stand-off distances. The design of the parameters table was created using Minitab 17's Box–Behnken Design method based on the four-factor three-level parameters utilized for the experiment. Table 3 lists the four parameters and the levels of each parameter used in the experiment, along with observed responses. The parameter combinations of all the experiments designed using the Box–Behnken method are listed in Table 4.

**Figure 2.** Microscopic view of SiC abrasive grits (a) 100 μm , (b) 150 μm , and (c) 200 μm size.**Table 3.** Process parameters and their levels.

Factors	Symbol	Minimum Value (−1)	Mean Value (0)	Maximum Value (+1)
Pressure (kg/cm^2)	p	4	6	8
Grain size (μm)	GS	100	150	200
Stand-off distance (mm)	SOD	24	28	32
Flow rate (g/min)	Q	120	130	140
Observed Responses		MRR	R_a (Arithmetic Average Roughness)	

Measurements of surface roughness were conducted using a surface roughness tester SURTRONIC 3+. In addition, a 3D surface profilometer (Taylor Hobson) was also utilized to analyze the topographic features of the surfaces. The morphology of the prepared surfaces was observed using an SEM (Evo 18 Research, Zeiss, Germany).

Table 4. Experimental results of *MRR* and arithmetic average *R_a* obtained on SS 304 sheet.

Sl. No.	Pressure (kg/cm ²)	Grain Size (μm)	Standoff Distance (mm)	Flow Rate (g/min)	<i>MRR</i> (g/min)	<i>R_a</i> (μm)
1	6	100	28	140	0.314000	0.775
2	8	150	24	130	0.388000	0.916
3	8	100	28	130	0.287850	1.203
4	8	150	28	140	0.383000	1.123
5	6	200	28	140	0.348000	1.146
6	6	100	24	130	0.341452	1.025
7	6	200	32	130	0.342804	1.153
8	4	150	28	140	0.339000	1.124
9	6	150	32	140	0.297000	1.220
10	8	200	28	130	0.383766	1.033
11	6	150	24	140	0.291667	0.921
12	4	150	24	130	0.375725	1.246
13	8	150	32	130	0.360314	0.791
14	6	100	28	120	0.352000	1.233
15	4	150	28	120	0.357000	0.816
16	6	150	24	120	0.341818	1.160
17	6	150	32	120	0.298156	1.280
18	6	150	28	130	0.382727	0.996
19	8	150	28	120	0.293254	1.109
20	4	100	28	130	0.382371	1.233
21	6	150	28	130	0.364545	0.740
22	6	200	28	120	0.345235	1.210
23	4	150	32	130	0.359000	0.728
24	6	200	24	130	0.348401	1.120
25	6	150	28	130	0.365455	0.827
26	4	200	28	130	0.367778	0.856
27	6	100	32	130	0.366765	0.857

3. Results and Discussion

The photographs of the prepared SS 304 work pieces $\sim(6 \times 3)$ mm² surfaces are shown in Figure 3. The dark areas at the centers of the specimen are the regions roughened using the abrasive particles.

3.1. Surface Characterization by SEM Analysis

The morphology of the SS 304 surface before and after abrasive jet bombardment is shown in Figure 4a and Figure 4b, respectively. A rough topography with traces of micro-indentations and shearing was observed on the workpiece after the impact of abrasive particles under high pressure. The random abrasive particles with sharp edges (Figure 2) cut through the surface, resulting in shearing off the material from the substrate surface (Figure 4a). In addition, the sharp edges of the abrasive particles penetrate the surface after the impingement and produce micro-indentations, as revealed in Figure 4b. Hence, micro-shearing and micro-indentations are the predominant modes of material erosion from the

surface of ductile material SS 304 under the action of abrasive particles. Similar observations were also made by Ghara et al. [8] and Rodriguez et al. [26] on some other metals.

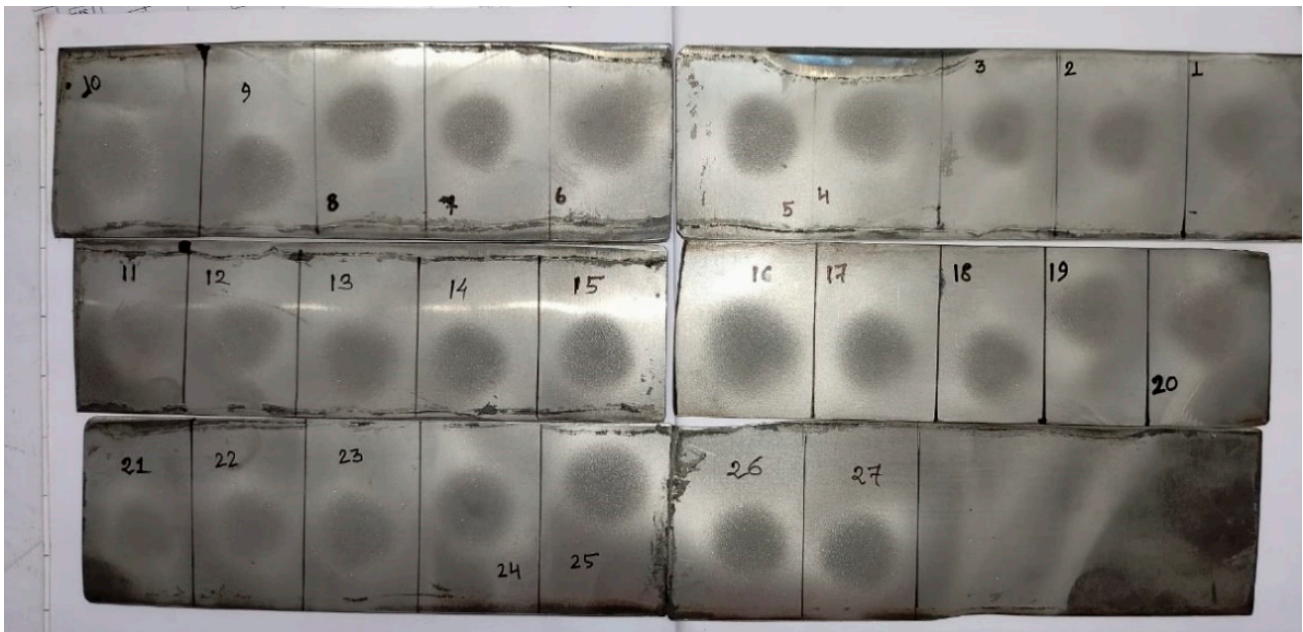


Figure 3. Inset photographs of the SS 304 specimens after surface roughening.

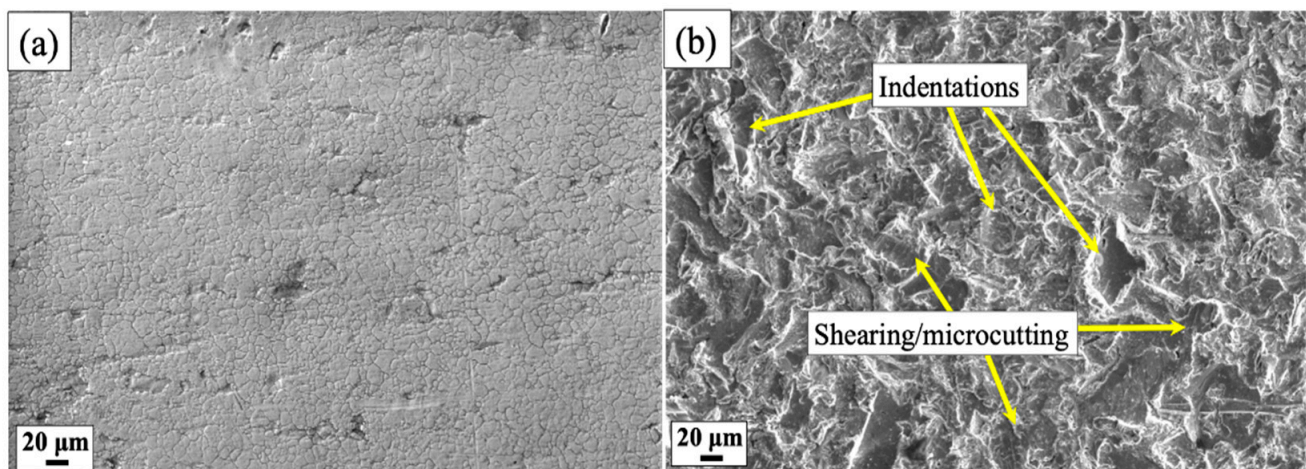


Figure 4. SEM micrographs of the SS 304 surface: (a) prior to and (b) after surface preparation at 8 kg/cm² pressure, 200 μm grit, 28 mm SOD, and 130 g/min abrasive flow rate.

3.2. Process Parameters Optimization

Table 4 lists the material removal rate (*MRR*) and average surface roughness of the specimens at different parameter combinations. The influence of individual and combined influence of process parameters on *MRR* is investigated using the analysis of variance (ANOVA) as presented in Table 5. The statistical analysis program Minitab 17 was used to tabulate the outcomes of the experiment.

The tests that were run are frequently summarized using an ANOVA table. It can be shown from Tables 5 and 6 that all of the terms related to the responses *MRR* and R_a in Equations (1) and (2) are significant because the *p*-values for these terms are less than 0.05. Table 6 shows the ANOVA table for the response surface quadratic model for material removal rate (*MRR*). The resulting models are regarded to be statistically significant, which is desired since it shows that the terms in the model have a substantial impact on the responses when the values of '*p*' (Prob. > *F*) in Table 6 for the term of models are less than

0.05 (i.e., =0.05, or 95% confidence). The other significant statistic, R^2 , which is referred to as determination coefficients in the final ANOVA table, is a measure of the degree of fit and is defined as the proportion of explained variance to total variation. The more closely the response model matches the real data, the more R^2 becomes close to unity. The obtained R^2 value (0.993) for MRR approaches to unity, suggesting that the experimental and predicted values are well-correlated. In Table 6, the calculated values of the F-ratio for lack of fit are compared with the standard values of the F-ratio corresponding to their degrees of freedom. The standard percentage point of F distribution for 95% confidence level is 3.74. However, the F value (3.14) for lack of fit is smaller than the standard value indicating that the model is adequate. Similarly, results from Table 6 indicate that the model is also significant, and it also displays that the test of lack-of-fit is insignificant. Because $F = 3.04 < 3.74$ ($F_{0.05,2,14} = 3.74$), a null hypothesis cannot be rejected, which means the model is adequate. It is also seen that there is a good correlation between the experimental and the predicted values due to the high R^2 value (0.965).

Table 5. Analysis of variance (ANOVA) table for MRR .

Source	DF	Seq SS	Adj SS	F	P	
Regression	10	0.024989	0.024989	226.66	0.000	Significant
Linear	4	0.022698	0.022698	514.71	0.001	
Square	3	0.002172	0.002172	65.67	0.000	
Interaction	3	0.000119	0.000119	3.59	0.037	
Residual Error	16	0.000176	0.000176			
Lack-of-Fit	14	0.000174	0.000174	3.15	0.103	Not significant
Pure Error	2	0.000003	0.000003			
Total	26	0.025165				
				R^2	0.993	
				R^2 (Adj)	0.989	

Table 6. Analysis of variance (ANOVA) table for R_a .

Source	DF	Seq SS	Adj SS	F	P	
Regression	10	0.808812	0.808812	44.33	0	Significant
Linear	4	0.445269	0.445269	61.01	0	
Square	3	0.244181	0.244181	44.61	0	
Interaction	3	0.119362	0.119362	21.81	0	
Residual Error	16	0.029193	0.029193			
Lack-of-Fit	14	0.028613	0.028613	3.04	0.131	Not significant
Pure Error	2	0.000581	0.000581			
Total	26	0.838005				
				R^2	0.965	
				R^2 (Adj)	0.943	

The final quadratic models of the response equation are presented as follows. The Regression Equation for MRR is given as:

$$MRR = -1.87 + 0.0872 p + 0.00258 GS + 0.0283 SOD + 0.0199 Q - 0.00603 p^2 - 0.000003 GS^2 - 0.000547 SOD^2 - 0.000069 Q^2 - 0.043 pGS + 0.00208 pSOD + 0.0057 pQ \quad (1)$$

$$R_a = 0.95 - 0.279 p + 0.01136 GS + 0.1 SOD - 0.0756 Q + 0.01817 p^2 - 0.00023 GS^2 - 0.00229 SOD^2 + 0.000255 Q^2 + 0.000437 pGS + 0.00162 pSOD + 0.00046 pQ \quad (2)$$

The normal probability plots of the residuals and the plots of the residuals vs. the predicted response for MRR and R_a are shown in Figures 5 and 6, respectively. According to a review of the plots in Figures 5a and 6b, the residuals typically fall on a straight line, indicating that the errors are distributed regularly. Additionally, Figures 5b and 6b reveal that they have no obvious pattern or unusual structure. This suggests that the offered models are suitable and that the assumptions of independence and constant variance have not been violated. The plots of main effects (Figures 7 and 8) are made to examine the

impacts of the parameters on the MRR and R_a respectively. As may be seen from Figure 7, pressure is the most significant factor in MRR , and grain size is the most significant factor for R_a .

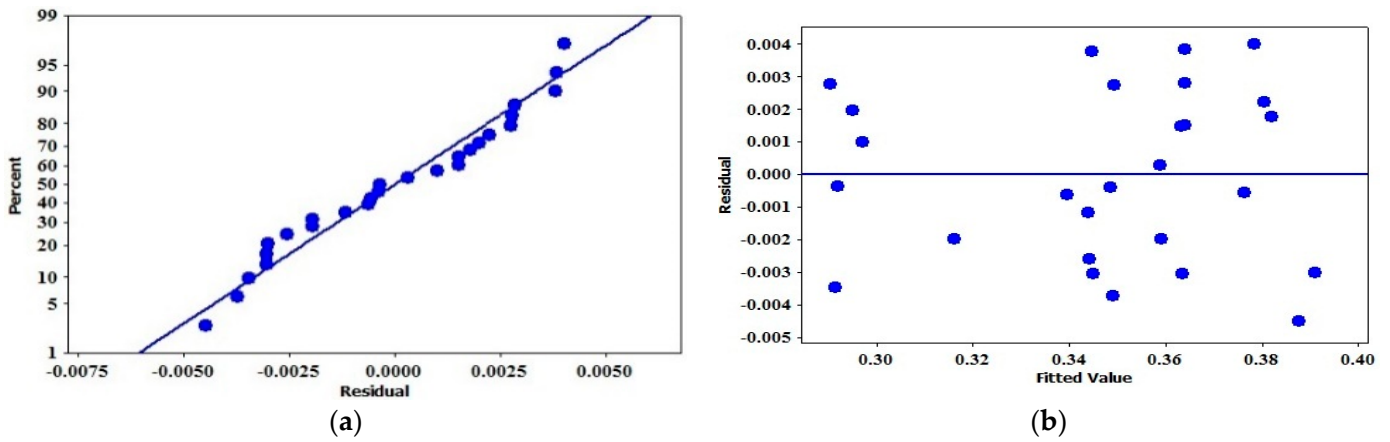


Figure 5. (a) Normal probability plot of residuals for MRR . (b) Plot of residuals vs. predicted response for MRR .

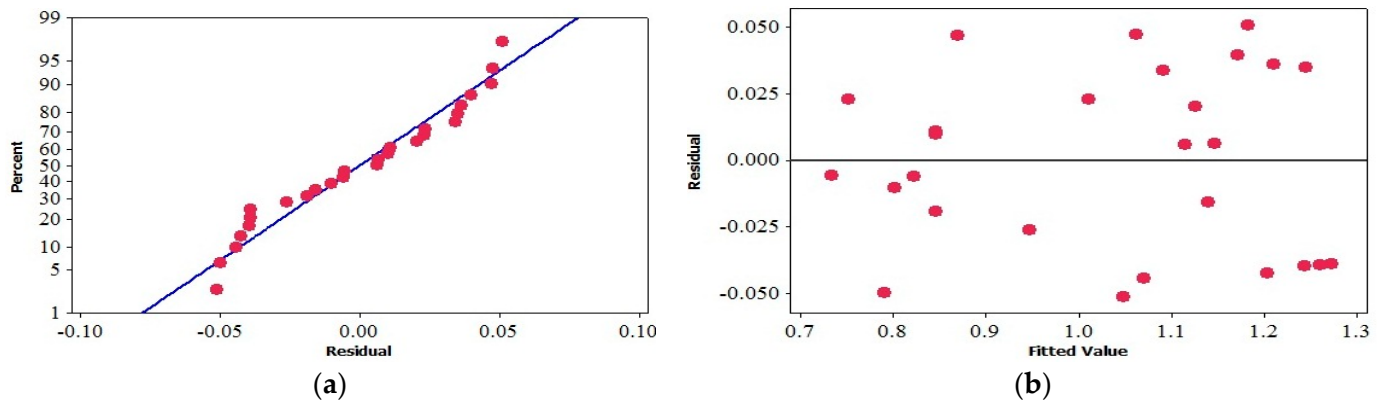


Figure 6. (a) Normal probability plot of residuals for R_a . (b) Plot of residuals vs. predicted response for R_a .



Figure 7. Mean effects plots of MRR .

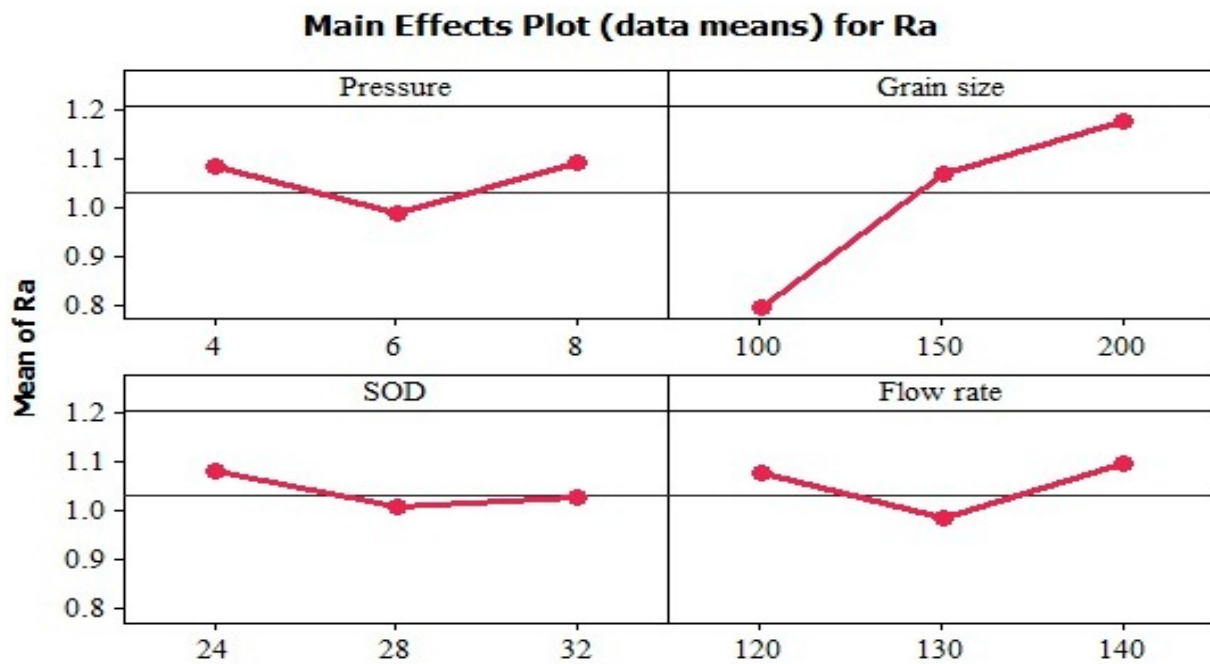


Figure 8. Mean effects plots of R_a .

Figure 9a–c indicate that MRR is highly influenced by working gas pressure, which is quite normal as high pressure enhances high kinetic energy to the abrasive jet stream and causes propionate MRR . Figure 9d–f show the effect of SiC abrasive grain size, flow rate, and SOD on MRR . In this range of study, lower grain size at intermediate SOD and flow rate provides higher MRR .

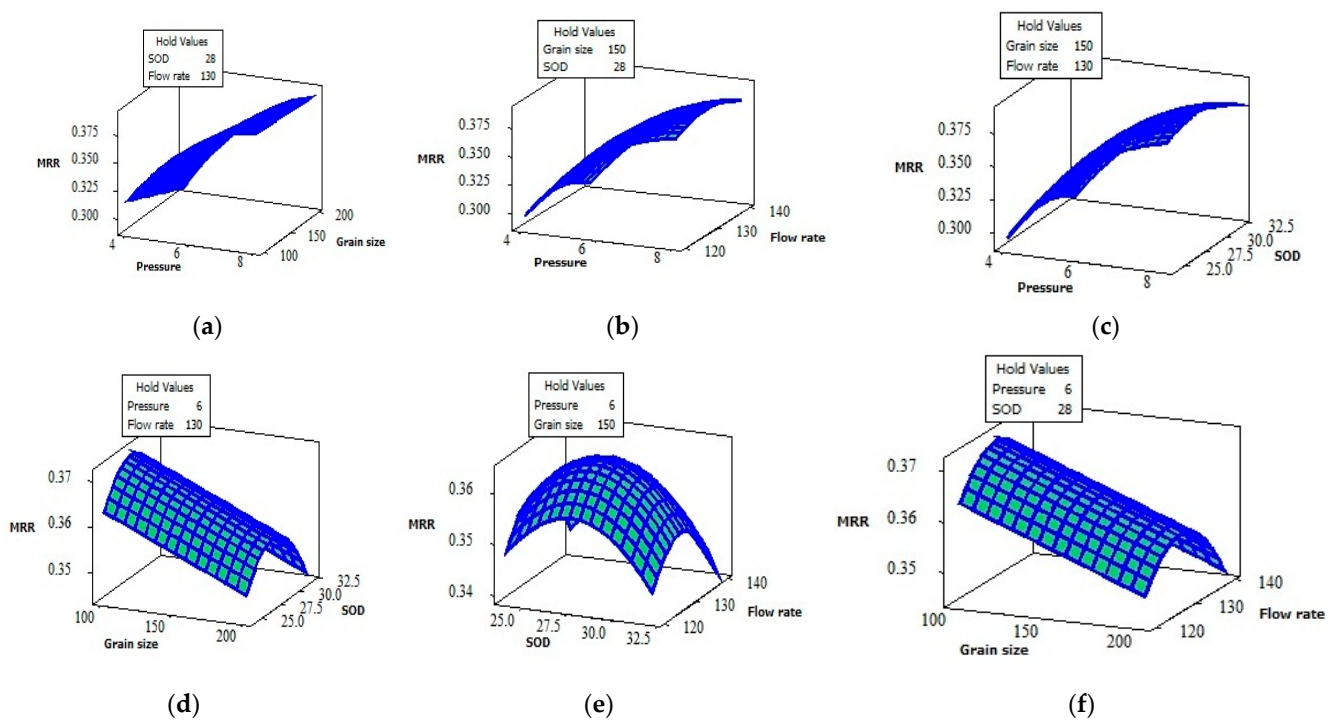


Figure 9. Surface plots (a–f) of MRR versus input parameters.

Figure 10a–c indicate that R_a values decrease and then increase with increasing working pressure. Roughening at low gas pressure might be due to the impingement of abrasive sharp edges in the SS 304 surface that might cause higher surface roughness with

lower metal removal. The SiC grain sizes show a major impact on R_a /roughening as in Figure 10d,e. In this range of study, the effect of SOD and flow rate has less significance on R_a .

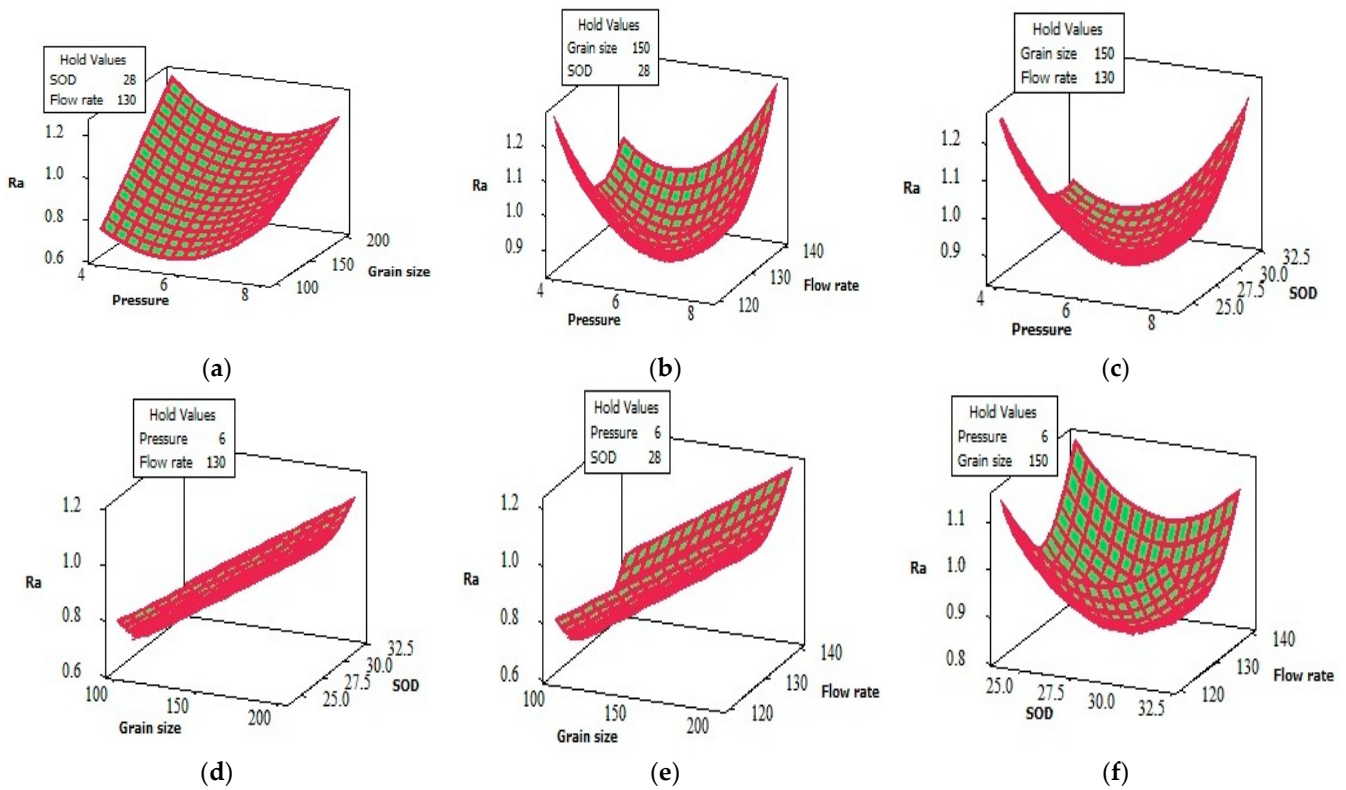


Figure 10. Surface plots (a–f) of R_a versus input parameters.

Here, an RSM-based desirability technique was used to optimize the input parameters (pressure, grain size, SOD, and flow rate). Utilizing the desirability function, multiple response optimizations were carried out to optimize the performance parameter, surface roughness (weight age-2), and reduce MRR (weight age-1). This method involves converting the response model (R) into d, which was then again aggregated to a composite desirability function (D), as shown in Figure 11. It has been noted that the desirability function for composites (0.99711) is very near to one. This indicates that the parameters seem to have been set for favorable results for each response.

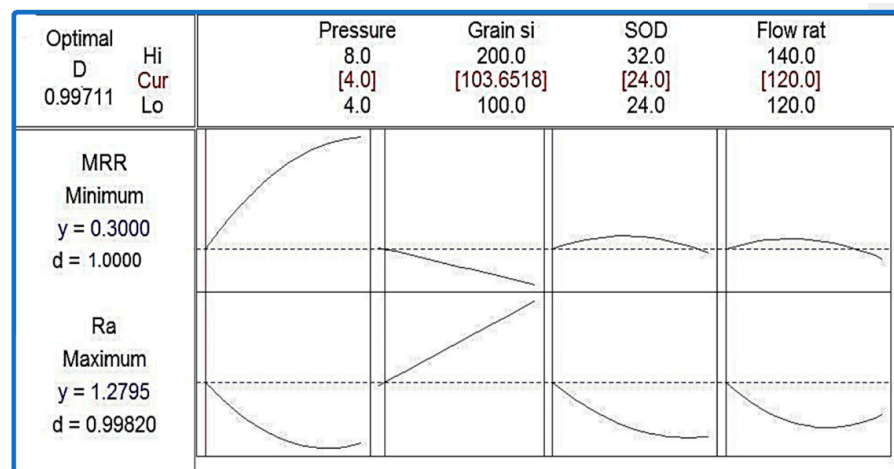


Figure 11. Desirability plot.

Good surface preparation is desirable without or with minimum *MRR*. To validate the optimization results, confirmation experiments were carried out using the following input parameters: pressure = 4 kg/cm², grain size = 100 μm, *SOD* = 24 mm, and flow rate = 120 g/min. Measurements were made of the corresponding responses (*MRR* and *R_a*). For a variety of responses, the RSM predictions agreed with the experimental average of 3 runs as shown in Table 7, which is shown numerically.

Table 7. Confirmation of optimization results.

Comparison	<i>MRR</i>	<i>R_a</i>
Predicted	0.300	1.2759
Experimental (experiment no.28 *)	0.3012	1.2543

where "*" indicates confirmation test/result.

The predicted value of *R_a* and *MRR* are very close to the experimental values. Therefore, the design of experiments, the experimental data analysis, and their trained/predicted value are very close to the real value. This model can be utilized for predicting any real *R_a* and *MRR* further within this range of experiments.

3.3. Confirmation Test

The variation between experimental and predicted responses (*R_a* and *MRR*) are shown in Figure 12a and Figure 12b (respectively).

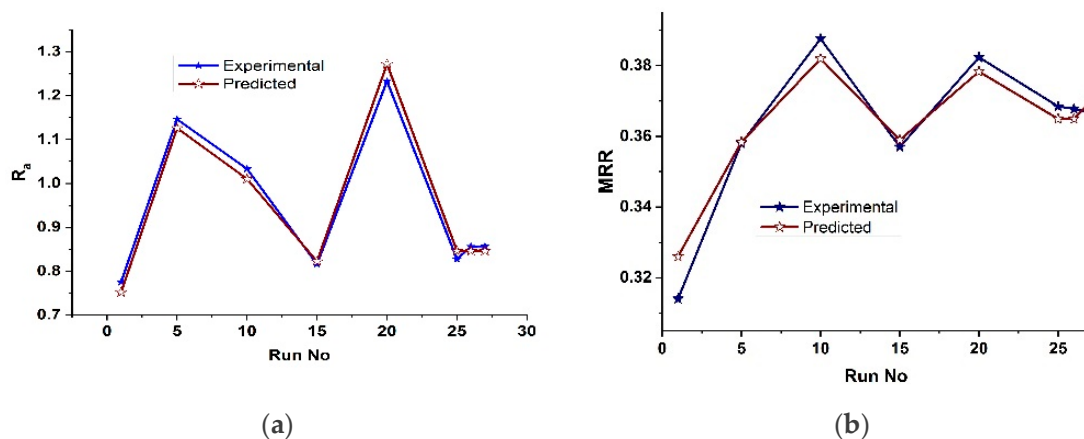


Figure 12. Comparison between experimental and predicted values for the (a) *R_a* and (b) *MRR*.

The result shows both the figures that predict values of the *MRR* and *R_a* close to recorded experimental values with a 95% confidence interval.

3.4. Sensitivity Analysis

To compare the estimated output to the measured data, model validation heavily relies on sensitivity analysis, a technique to determine essential factors and rank them according to importance. Mathematically, the sensitivity of a design objective function with respect to a design variable is the partial derivative of that function with respect to its variables. To obtain the sensitivity equations for *MRR* and *R_a*, Equations (1) and (2) are differentiated with respect to pressure. The sensitivity Equations (3)–(6) and Equations (7)–(10) represent the sensitivity of *MRR* and *R_a* for pressure, particle size, *SOD*, and flow rate, respectively.

$$\frac{\partial(MRR)}{\partial p} = 0.0872 - 0.0121p - 0.043S + 0.00208D + 0.0057F \quad (3)$$

$$\frac{\partial(MRR)}{\partial S} = 0.00258 - 0.00006S - 0.043p \quad (4)$$

$$\frac{\partial(MRR)}{\partial D} = 0.0282 - 0.0011D + 0.00208p \tag{5}$$

$$\frac{\partial(MRR)}{\partial F} = 0.0199 - 0.000138F + 0.0057p \tag{6}$$

$$\frac{\partial R_a}{\partial p} = -0.279 + 0.03634p + 0.00044S + 0.00162D + 0.0046F \tag{7}$$

$$\frac{\partial R_a}{\partial S} = 0.01136 - 0.0046S + 0.00044p \tag{8}$$

$$\frac{\partial R_a}{\partial D} = 0.1 - 0.00458D + 0.00162p \tag{9}$$

$$\frac{\partial R_a}{\partial F} = -0.0756 + 0.00051F + 0.00046p \tag{10}$$

This study aimed to predict the tendency of *MRR* and *R_a* due to changes in process parameters for surface preparation. Sensitivity of *MRR* and *R_a* to pressure, grain size, SOD, and flow rate, as calculated from Equations (3)–(6) and Equations (7)–(10), are reflected in Figure 13, respectively.

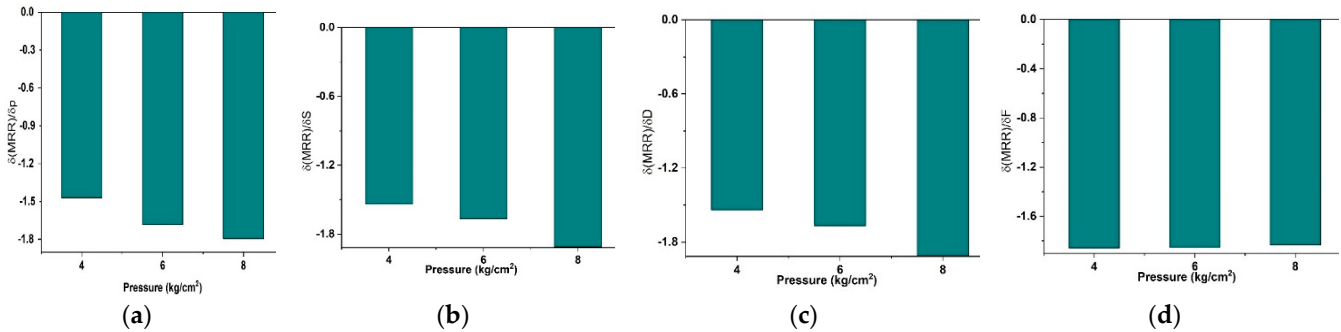


Figure 13. Sensitivity analysis result on MRR: (a) pressure, (b) grain size (c) SOD, and (d) flow rate.

The MRR was found (Figure 13a–d) to be more sensitive with respect to pressure, grain size, and SOD with a little variation in pressure. Rather, *R_a* was found (Figure 14a–d) to be more sensitive with respect to pressure and grain size with little pressure variation. From the overall observations, the pressure and grain size were found to be two main factors in the erosion MRR of SS 304. Ramachandran, C.S. et al., 2012 [31] recognized that

$$\text{Erosion} = \{K \times (\text{velocity})^n\} \tag{11}$$

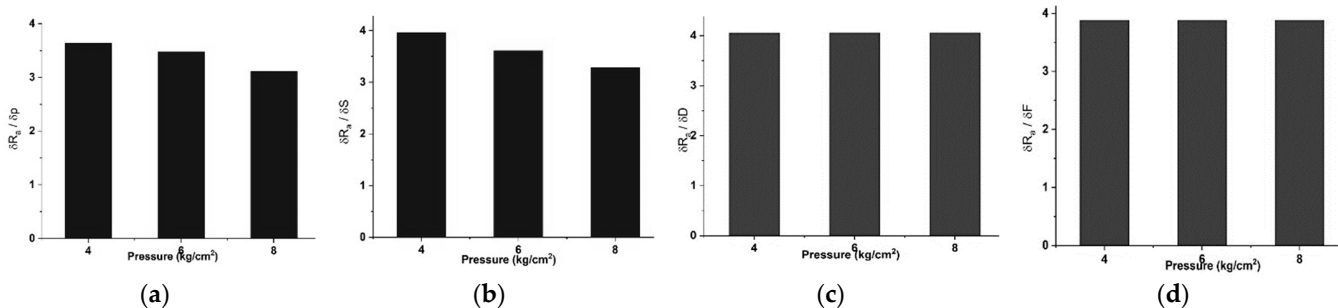


Figure 14. Sensitivity analysis result of *R_a* (a) pressure, (b) grain size, (c) SOD, and (d) flow rate.

‘*n*’ is a velocity exponent and ‘*K*’ is a constant that depends upon impact angle and particle size. To form an abrasive jet, the gas pressure head was converted to the velocity head which moves the gas-suspended abrasives. The kinetic energy of the abrasive erodes the material body if it is being impacted. Therefore, Equation (11) supports the findings of the present study.

The expert's studies [31,32] are based on the air-jet erosion tester which can possibly measure the particle velocity before erosion impact which has made the explanation of erosion easier. In general, industrial air-jet systems are used in various applications without such instruments to reduce additional costs. The air-jet process parameters like pressure, nozzle diameter, *SOD*, etc., could be synchronized with erosion–velocity empirical relation (Equation (5)), which may give more benefits for industrial users.

3.5. 3D Profilometry Analysis for Surface Quality Characterization

A rough surface consists of multiple peaks, valleys, and flats. Therefore, the topography of the surface can be characterized based on two important parameters, namely the sharpness of the peaks (S_{ku}) (Kurtosis) and the density of peaks (S_{pd}) on a particle surface. S_{ku} is a measure of the sharpness of the peaks present on a rough surface. Figure 15 schematically depicts different types of peaks and corresponding S_{ku} values [33]. When $S_{ku} < 3$, the height distribution, is skewed and the peak is represented as a hump, at $S_{ku} = 3$, the height distribution above the mean plane followed a normal distribution. A sharply spiked height distribution is assumed for a $S_{ku} > 3$. On the other hand, the quantity of peaks per unit area is represented as S_{pd} (density of peaks). Another parameter that represents the sharpness of the peaks is the Arithmetic mean peak curvature (S_{pc}). A larger value of S_{pc} means the curvature of the peaks are smaller, i.e., the peaks are sharper. A smaller value of S_{pc} indicates wider curvature of the peaks.

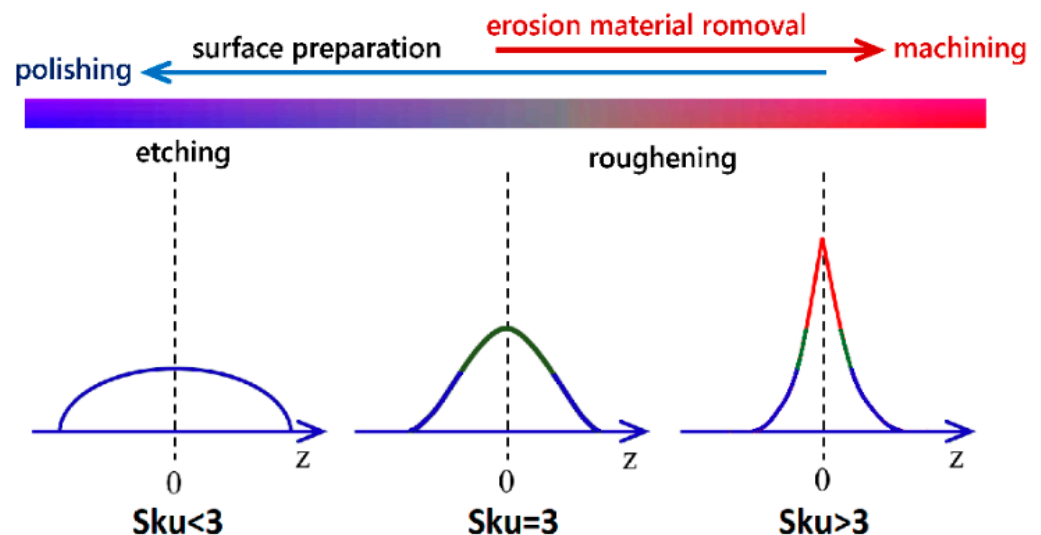


Figure 15. Schematic representation of the profiles of peaks indicating sharpness parameter (S_{ku}), related to surface preparation and erosion material removal.

For the detailed analysis of the surface topography characteristics (S_{ku}, S_{pd}), eight specimens (sl.no. 2, 6, 19, 20, 24, and 28 * from Table 3) are selected. The measured values of S_{ku}, S_{pd} of the selected specimens are presented in Table 8.

The 3D images of the surface topography corresponding to sl. no. 1 to 6* (in Table 8), obtained using the 3D profilometer, are shown in Figure 16a–f, respectively. It is clear from Figure 16a,b that at higher pressure (8 kg/cm²), the prepared surface peaks are relatively flat and a few higher peaks are observed. It might be due to material removal being the main mood of abrasion instead of surface roughening.

Table 8. Surface topography parameters (S_{ku} , S_{pd} , S_{pc}) measured using 3D profilometer.

Sl. No.	Figure No.	Pressure (kg/cm ²)	Grain Size (μm)	SOD (mm)	Flow Rate (g/min)	S_{ku} (Kurtosis)	S_{pd} (Density of Peaks) (1/mm ²)	R_a (μm)	S_{pc} (Arithmetic Mean Peak Curvature) (1/mm)
1	16a	8	150	24	130	3.51	39.2	0.916	21.4
2	16b	8	100	24	130	3.38	37.9	1.025	15.9
3	16c	6	150	28	120	3.37	46	1.109	17.6
4	16d	4	100	28	130	3.42	49.1	1.233	16.7
5	16e	4	200	24	130	4.33	25.9	1.120	27.1
6*	16f	4	100	24	120	3.45	51.2	1.254	16.2

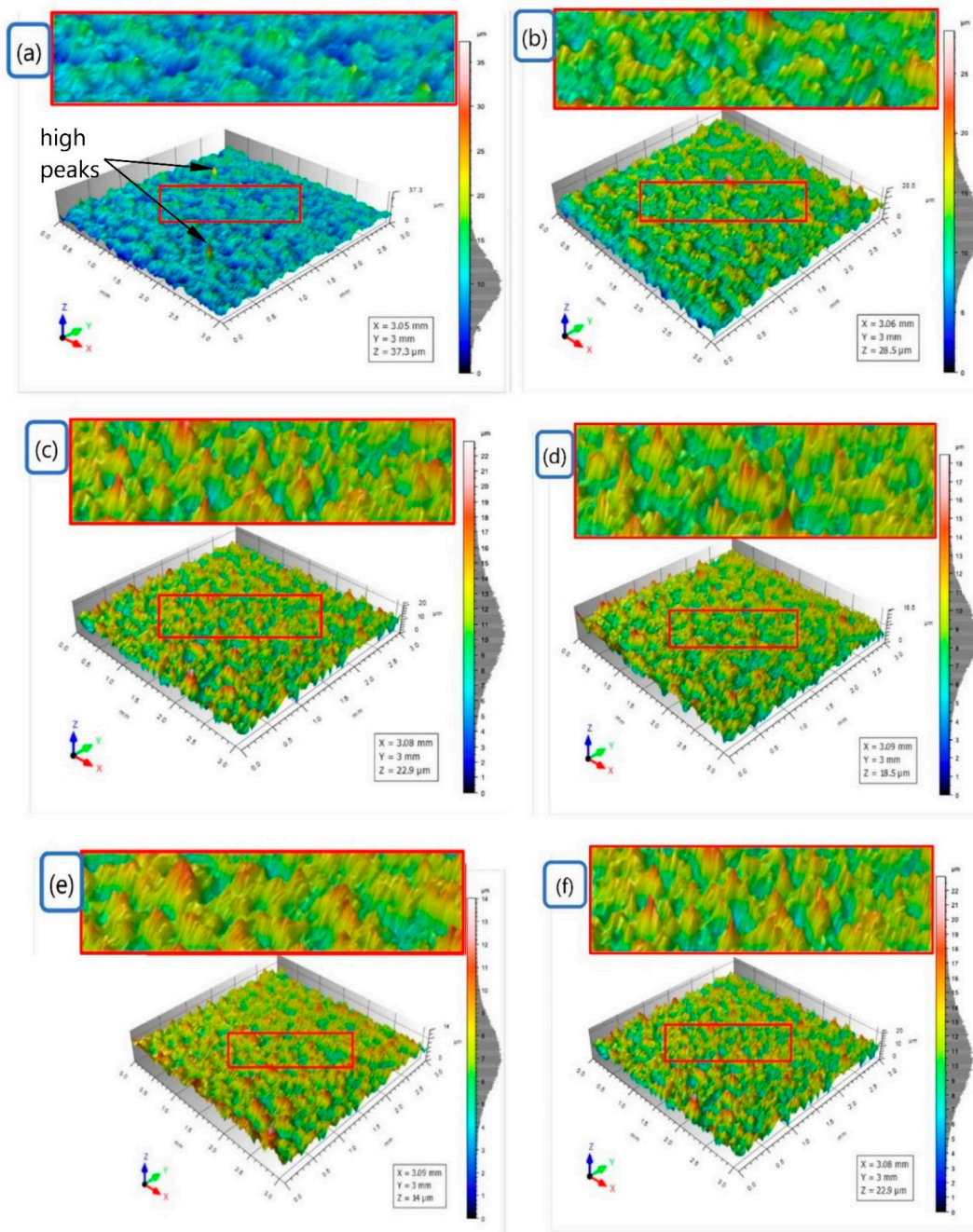


Figure 16. 3D surface topography obtained at (a–e) as per designed experimental input parameters, and (f) as per predicted process parameters.

The surface topography at medium pressure (6 kg/cm²) in Figure 16c indicates an intermediate level of surface preparation. Figure 16d–f exhibit peaks that are relatively more prominent and sharper, indicating that the surface topography is better at minimum gas pressure (4 kg/cm²). It indicates that the indentation of sharp SiC grits is the main mechanism to create sharp peaks on the SS 304 work surface.

4. Conclusions

The effects of process parameters on both abrasive jet surface preparation and erosion material removal were investigated, analyzed, and the observations are concluded as follows:

- In the surface preparation of SS 304, abrasive (SiC) grain size was one of the significant process parameters. The working gas pressure plays a typical role in surface preparation at a minimum pressure (4 kg/cm²). The roughness profile peaks were found to be very sharp ($S_{ku} > 3$) and higher in density (S_{kpd}) in this condition.
- In erosion material removal, the maximum MRR was found at maximum working gas pressure (8 kg/cm²).
- The regression coefficient was used to develop the mathematical (quadratic) models of two responses (MRR and R_a), and ANOVA was used to determine their statistical significance for each output response. The model has been determined to be statistically significant because the values of p were less than 0.05.
- The operating conditions were optimized as pressure 4kg/cm², grain size ~100 μm, SOD 24 mm, and flow rate 120 g/min, where maximum surface roughness at minimum MRR was obtained using D-optimal test with composites desirability of 0.9971.
- SEM view, 3D profilometry view, and analysis proved that the material deformation, indentation, erosion, etc., were the main mechanisms in SiC air jet bombardment on SS 304.
- The sensitivity analysis revealed that gas pressure was the most significant factor in influencing the responses.

Author Contributions: Conceptualization, S.D. and B.H.; methodology, V.P. and D.K.A.; software, H.J.; validation, V.P., H.J. and B.H.; formal analysis, V.P. and D.K.A.; investigation, V.P., D.K.A., S.D. and T.G.; resources, S.D. and T.G.; data curation, V.P.; writing—original draft preparation, V.P., T.G., B.H. and H.J.; writing—review and editing, B.H., S.D., H.J. and T.G.; visualization, B.H., S.D., H.J., N.A. and T.G.; supervision, B.H. and S.D.; project administration, B.H. and S.D.; funding acquisition (for internal expenditure), B.H. and N.A. All authors have read and agreed to the published version of the manuscript.

Funding: This research received no external funding.

Data Availability Statement: Data may be available upon request to the corresponding author.

Acknowledgments: The authors are thankful to Kalyani Government Engineering College, Kalyani, India for providing all sorts of support needed for carrying out the experimental investigation. They also thank the Dean of Scientific Research, Imam Mohammad Ibn Saud Islamic University (IMSIU), Riyadh, Saudi Arabia for extended support in this investigation.

Conflicts of Interest: The authors declare no conflict of interest.

Nomenclature

MRR	Material removal rate in (g/min)
SEM	Scanning electron microscope
SiC	Silicon carbide
AJM	Abrasive jet machining
AWJM	Abrasive water jet machining
p	Pressure (kg/cm ²)
GS	Grain size (μm)

SOD	Stand-off distance (mm)
Q	Flow rate (g/min)
ANOVA	Analysis of variance
R_a	Surface roughness in μm
RSM	Response surface method
S_{pd}	Density of peaks
S_{ku}	Sharpness of the peaks

References

- Haldar, B.; Adak, D.K.; Ghosh, D.; Karmakar, A.; Habtamu, E.; Ahmed, A.; Das, S. Present status and some critical issues of abrasive jet materials processing: A review. *Procedia Manuf.* **2018**, *20*, 523–529. [[CrossRef](#)]
- Hebda, M.; Kaczor, P.; Miernik, K. Vacuum brazing of stainless steel depending on the surface preparation method and temperature of the process. *Arch. Metall. Mater.* **2019**, *64*, 5–11. [[CrossRef](#)]
- Lankiewicz, K.; Babul, T.; Baranowski, M.; Kowalski, S. The study of the impact of surface preparation methods of Inconel 625 and 718 nickel-base alloys on wettability by BNi-2 and BNi-3 brazing filler metals. *Arch. Metall. Mater.* **2015**, *60*, 739–745. [[CrossRef](#)]
- Thakare, G.J.; Pandey, C.; Mulik, S.R.; Mahapatra, M.M.; Narang, K.H. Effect of grit blasting and thermal spraying on microstructure evolution of P91 weldment. *Arch. Metall. Mater.* **2018**, *63*, 1725–1734. [[CrossRef](#)]
- Melentiev, R.; Fang, F. Recent advances and challenges of abrasive jet machining. *CIRP J. Manuf. Sci. Technol.* **2018**, *22*, 1–20. [[CrossRef](#)]
- Adnan, A.; Kulekci, K.M.; Seker, U.; Ercan, F. Effect of feed rate on surface roughness in abrasive water jet cutting applications. *J. Mater. Process. Technol.* **2004**, *147*, 389–396. [[CrossRef](#)]
- Ghara, T.; Paul, S.; Bandyopadhyay, P.P. Influence of grit blasting on residual stress depth profile and dislocation density in different metallic substrates. *Metall. Mater. Trans.* **2020**, *52*, 65–81. [[CrossRef](#)]
- Ghara, T.; Paul, S.; Bandyopadhyay, P.P. Effect of grit blasting parameters on surface and near-surface properties of different metal alloys. *J. Therm. Spray Technol.* **2020**, *30*, 251–269. [[CrossRef](#)]
- Parikshit, D.A.; Dubey, S.; Yogesh, D.V.; Abul, A.B.; Purushottam, B.S. Modelling and multi-objective optimization of surface roughness and kerf taper angle in abrasive water jet machining of steel. *J. Braz. Soc. Mech. Sci. Eng.* **2018**, *40*, 259. [[CrossRef](#)]
- Chaitanya, K.A.; Kishore, D.B.; Girish, K.K. Experimental study on surface roughness by using abrasive jet machine. *Mater. Today Proc.* **2020**, *23*, 453–457. [[CrossRef](#)]
- Tsai, C.F.; Yan, H.B.; Kuan, Y.C.; Huang, Y.F. A taguchi and experimental investigation into the optimal processing conditions for the abrasive jet polishing of SKD61 mold steel. *Int. J. Mach. Tools Manuf.* **2008**, *48*, 932–945. [[CrossRef](#)]
- Kim, A.; Kainuma, S.; Yang, M. Surface characteristics and corrosion behavior of carbon steel treated by abrasive blasting. *Metals* **2021**, *11*. [[CrossRef](#)]
- Chander, P.K.; Vashista, M.; Sabiruddin, K.; Paul, S.; Bandyopadhyay, P.P. Effects of grit blasting on surface properties of steel substrates. *Mater. Des.* **2009**, *30*, 2895–2902. [[CrossRef](#)]
- Bañon, F.; Sambruno, A.; Batista, M.; Simonet, B.; Salguero, J. Surface quality and free energy evaluation of s275 steel by shot blasting, Abrasive Water Jet Texturing and Laser Surface Texturing. *Metals* **2020**, *10*, 290. [[CrossRef](#)]
- Miturska-Barańska, I.; Rudawska, A.; Doluk, E. The influence of sandblasting process parameters of aerospace aluminium alloy sheets on adhesive joints strength. *Materials* **2021**, *14*, 6626. [[CrossRef](#)]
- Jagannatha, N.; Hiremath, S.S.; Sadashivappa, K. Analysis and parametric optimization of abrasive hot air jet machining for glass using taguchi method and utility concept. *Int. J. Mech. Mater. Eng.* **2012**, *7*, 9–15.
- Pradhan, S.; Das, R.S.; Nanda, K.B.; Jana, C.P.; Dhupal, D. Experimental investigation on machining of hardstone quartz with modified ajm using hot silicon carbide abrasives. *J. Braz. Soc. Mech. Sci. Eng.* **2020**, *42*, 559. [[CrossRef](#)]
- Jafar, R.; Mohammad, H.; Spelt, J.K.; Papini, M. Surface roughness and erosion rate of abrasive jet micro-machined channels: Experiments and analytical model. *Wear* **2013**, *303*, 138–145. [[CrossRef](#)]
- Nayak, B.B.; Kumar, A.; Mahapatra, S.S.; Das, D. Application of wpca based taguchi method for multi-response optimization of abrasive jet machining process. *Mater. Today Proc.* **2018**, *5*, 5138–5244. [[CrossRef](#)]
- Made, S.; Balasubramanian, M. Impact of nozzle design on surface roughness of abrasive jet machined glass fibre reinforced polymer composites. *Silicon* **2018**, *10*, 2453–2462. [[CrossRef](#)]
- Wakuda, M.; Yamauchi, Y.; Kanzaki, S. Surface finishing of alumina ceramics by means of abrasive jet machining. *J. Am. Ceram. Soc.* **2002**, *85*, 1306–1308. [[CrossRef](#)]
- Ke, J.H.; Tsai, F.C.; Hung, J.C.; Yan, B.H. Characteristics study of flexible magnetic abrasive in abrasive jet machining. *Procedia CIRP* **2012**, *1*, 679–680. [[CrossRef](#)]
- Slatineanu, L.; Dodun, O.; Nagit, G.; Coteata, M.; Coteata, L.; Tabacaru, L.; Bancescu, B. Evaluation of the surface profile obtained by abrasive jet machining. *IOP Conf. Ser. Mater. Sci. Eng.* **2018**, *444*, 032005. [[CrossRef](#)]
- Kwon, D.K.; Lee, J.H. Performance Improvement of micro-abrasive jet blasting process for Al 6061. *Processes* **2022**, *10*, 2247. [[CrossRef](#)]
- Sanghani, S.; Chirag, R.; Korat, M.M. Performance analysis of abrasive water jet machining process for AISI 304 stainless steel. *J. Exp. Appl. Mech.* **2017**, *8*, 53–55.

26. Wang, W.; Biermann, D.; Almuth, R.; Arif, M.F.A.; Veldhuis, C.S. Effects on tool performance of cutting edge prepared by pressurized air wet abrasive jet machining (PAWAJM). *J. Mater. Process. Technol.* **2020**, *227*, 116–456. [[CrossRef](#)]
27. Ficko, M.; Begic-Hajdarevic, D.; Husic, M.C.; Berus, L.; Cekic, A.; Klančnik, S. Prediction of surface roughness of an abrasive water jet cut using an artificial neural network. *Materials* **2021**, *14*, 3108. [[CrossRef](#)]
28. Hlaváčová, I.M.; Sadílek, M.; Váňová, P.; Szumilo, Š.; Tyč, M. Influence of steel structure on machinability by abrasive water jet. *Materials* **2020**, *13*, 4424. [[CrossRef](#)]
29. Steel, S.; Graphs, M. Machinability of Stainless Steel. Available online: <https://www.machiningdoctor.com/machinability/stainless-steel-2/> (accessed on 17 October 2022).
30. Charles, J. Past, Present and Future of the Duplex Stainless Steels. Available online: <https://www.worldstainless.org/Files/issf/non-image-files/PDF/Pastpresentandfutureoftheduplexstainlesssteels.pdf> (accessed on 10 October 2022).
31. Ramachandran, C.S.; Balasubramanian, V.; Ananthapadmanabhan, P.V. Erosion of atmospheric plasma sprayed rare earth oxide coatings air-suspended corundum particles. *Ceram. Int.* **2013**, *39*, 649–672. [[CrossRef](#)]
32. Mahade, S.; Venkat, A.; Curry, N.; Leitner, M.; Joshi, S. Erosion performance of atmospheric plasma sprayed thermal barrier coatings with diverse porosity levels. *Coatings* **2021**, *11*, 86. [[CrossRef](#)]
33. Keyence Corporation. Area Roughness Parameters. Available online: <https://www.keyence.com/ss/products/microscope/roughness/surface/sku-kurtosis.jsp> (accessed on 10 October 2022).

Disclaimer/Publisher’s Note: The statements, opinions and data contained in all publications are solely those of the individual author(s) and contributor(s) and not of MDPI and/or the editor(s). MDPI and/or the editor(s) disclaim responsibility for any injury to people or property resulting from any ideas, methods, instructions or products referred to in the content.